# Excitonic switching across a Z 2 topological phase transition: From Mott-Wannier to Frenkel excitons in organic materials

D. Romanin, M. Calandra, Alex W. Chin

# Excitonic switching across a $Z_2$ topological phase transition: from Mott-Wannier to Frenkel excitons in organic materials

D. Romanin,[1,*] M. Calandra,[2,1,†] and A. W. Chin[1,‡]

[1] *Sorbonne Université, CNRS, Institut des Nanosciences de Paris, UMR7588, F-75252, Paris, France*
[2] *Department of Physics, University of Trento, Via Sommarive 14, 38123 Povo, Italy*

(Dated: November 22, 2022)

Controllable topological phase transitions in low dimensional materials allows for unconventional optical selection rules and exciton series. We show that the broad mixing of single-particle contributions to the exciton states occurring across a $Z_2$ phase transition in 1D polyacene polymers leads to an extreme tunability of optical properties, with exciton dispersions ranging from gigantic bandwidth ($\approx 1.5$ eV) to practically zero. The acene length transversal to the periodic axis controls the exciton localization, allowing for a cross-over from Mott-Wannier to Frenkel-like excitons and large changes in optical gaps, singlet-triplet splittings and the orbital structure of the real-space exciton states. Our work opens appealing perspectives for the design of novel optolectronic devices.

## I. INTRODUCTION

Band topology is now considered to be as fundamental as band structure [1, 2], underlying emergent quasiparticle phenomena such as robust edge states and spin-chain physics in organic systems (e.g. graphene nanoribbons) [3–5]. Moreover, the impact of topological band structures on the physics of excitons (i.e. an electron-hole photo-excited state bound by Coulomb interaction) has attracted a lot of attention in the last decade [6–17]. As a matter of fact, it has been shown for low dimensional materials that band topology dramatically changes their photophysics, breaking conventional optical selection rules and leading to novel exciton series [18, 19]. Thus, understanding and controlling the effects of topological phase transitions on the optical response of materials represents a new powerful tool for the design of novel optoelectronic devices.

Generally speaking, $\pi$-conjugated organic semiconductors form a highly promising class of materials for the development of cheap, flexible and non-toxic optoelectronic devices such as photovoltaics, sensors and solid state lighting [20, 21]. Experimental evidence for a topological ($Z_2$) *phase transition* has recently been presented in a series of $1D$ polyacene polymers in which the monomer size and chain length could be systematically varied [22, 23], representing a physical realization of the well known Su-Schrieffer-Heeger (SSH) model [1]. This transition is associated with a dramatic closing and reopening of the polymer quasiparticle gap, as the size of the monomer increases. Nevertheless, the effects of a topological phase transition on the photophysics of such low-dimensional organic systems has, to date, remained unexplored and, based on the discussion above, could be relevant for the design of future carbon-based optoelectronic devices.

Figure 1 shows the structure of the polyacene polymers

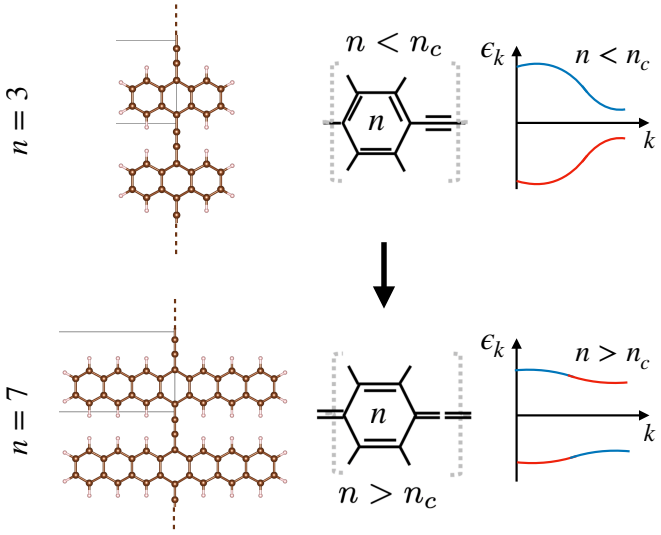


FIG. 1. Topological phase transition of polyacene polymers: as the acene length $n$ increases, the bridge configuration switches from ethylnic ($-C \equiv C-$) to cumulenic ($= C = C =$), while the central ring goes from an aromatic to a quinoidal form. Above a critical length $n_c$, the topologically non-trivial phase (see text) emerges, showing a smooth change of orbital character (red,blue) across the Brillouin zone (band inversion).

of Ref. [22], which are composed by acene monomers connected by ethynylene bridges. The number of aromatic rings in each monomer is labeled $n$. Experimental chain lengths for both anthracene ($n = 3$) and pentacene ($n = 5$) vary from a few to a few-hundred monomers in the bridge direction (one dimensional periodicity). The HOMO-LUMO gap for acene monomers decreases smoothly as $n$ increases, tending to a finite limit as $n \to \infty$ [24]. However, it was observed in Refs. [22, 23] that the band gap in polyacene polymers on Au(111) almost closes completely when going from $n = 3$ (anthracene) to $n = 5$ (pentacene). STM images revealed this to be accompanied by a marked change in the bond-length alternation (BLA, defined as the difference be-

* romanin@insp.jussieu.fr
† m.calandrabuonaura@unitn.it
‡ chin@insp.jussieu.fr

tween the single and triple bond lengths in the ethynylene link) of the polymer bridges, as well as a transition from an aromatic to quinoidal configuration for the central carbon rings in the monomers (Fig. 1). Crucially, these observations were rationalized in Ref. [22, 23] by relating the electronic structure of the polymers to an effective Su-Schreiffer-Heeger (SSH) model [1]. The rationale for this correspondence is summarized in the Supplemental Material [25] (SM, Sec. S2), but the key point is that this well-known model possesses a $Z_2$ topological phase transition as the ratio $t_1/t_2$ between the intra- (HOMO-LUMO gap, $t_1$) and inter-monomer (bridge-mediated, $t_2$) electron hopping amplitudes is tuned. Changing $n$, and thus $t_1$, allows the polymers to cross the transition. The topological nature of the $n = 5$ acene polymers was further confirmed by the detection of localized 'edge states' in sufficiently long-but-finite pentacene ($n = 5$) polymers, as well as band inversion (*vide infra*) of their conduction and valence states [22, 23].

In this paper, by employing manybody perturbation theory, we investigate the excitonic properties across the $Z_2$ topological transition occurring in polyacene polymers. We show that the topological transition is accompanied by a switching from extended Mott-Wannier excitons to localized Frenkel excitations and exciton dispersions that can be tuned from gigantic bandwidth ($\approx 1.5$ eV) to practically zero, simply by controlling the acene length $n$ (see Fig. 1). This extreme tunability of optical properties occurs whilst also maintaining the desirable characteristics (large binding energy, strong optical absorption, large singlet-triplet splittings) that make organics attractive for applications [26]. Even more strikingly, we also show that a defining feature of non-trivial band topology - band inversion - can be seen directly in the experimentally measurable real-space wave functions of the excitons [27].

In Sec. II we summarize the computational details both for the structural, electronic (Sec. II A) and optical (Sec. II B) properties. We then discuss in the detail in Sec. III A the electronic band structure in vacuum of the various polymers under study (i.e. $n = 3, 5, 7$) and in Sec. III B we also analyze the effect due to the screening of the environment. After that, in Sec. III B and Sec. III C we analize the effects of the topological phase transition on the exciton wavefunctions and their dispersion respectively. In Sec. III D we study the origin of a negative dispersive triplet close to and after the quantum critical point of the topological phase transition. Finally, in Sec. IV we report our conclusions.

## II. COMPUTATIONAL METHODS

### A. Structural and electronic properties

Density functional theory calculations on the ground-state geometry (i.e. unit cell and atomic positions) are performed in vacuum with localized gaussian basis, using CAMB3LYP hybrid xc functional [28, 29] and CRYSTAL17 [30, 31]. The CAMB3LYP hybrid functional includes long-range corrections to the B3LYP, which is particularly suited for carbon-based materials, and has been shown to provide accurate results for charge transfer excitations, excitations to Rydberg states, polarizability of long chains and vibrational properties comparable to those obtained via Quantum Montecarlo methods [32, 33] for systems in vacuum. We have employed the triple-ξ-polarized Gaussian type basis set[34] with real space integration tolerances of 10-10-10-25-50 and an energy tolerance of $10^{-12}$ Ha for the total energy convergence. Each polymer has its principal axis along the $x$ direction, with $\sim$ 500 Å of vacuum along the non-periodic $y$ and $z$ directions in order to have a proper one-dimensional system. The Brillouin zone is sampled with a uniform mesh of $50 \times 1 \times 1$ k-points. Relaxation of the atomic coordinates is performed by imposing the polymers to be flat, since they have been synthesized on a surface. The out-of-plane relaxation is discussed in the SM [25] (Sec. S3). Finally, we consider here a paramagnetic ground state. The possible occurrence of magnetic states at very low temperature [35, 36] is discussed in the SM [25] (Sec. S5), which however does not hinder the results presented here.

### B. Optical properties

Many-body corrections to the single-particle band-structure are computed within the GW approximation using the Yambo [37, 38] code and the plasmon-pole approximation [39]. Eigenvalues and wavefunctions are initially computed with the Perdew-Burke-Ernzerhof (PBE) exchange-correlation (xc) functional and Quantum ESPRESSO [40, 41]. Each polymer has its principal axis along the $x$ direction, with $\sim$ 10 Å of vacuum along the non-periodic $y$ and $z$ directions as well as a cut-off on the Coulomb potential [42] in order to have a proper one-dimensional system. In this case we have employed a norm-conserving pseudopotential with the kinetic energy cut-off set to 70 Ry and a threshold of $10^{-10}$ Ry on the total energy.

We performed self-consistent $GW$ calculations on eigenvalues only (ev$GW$) [43] for both the Green's function $G$ and the screened electron-electron interaction $W$ in the Plasmon-Pole approximation (PPA). Excitonic effects are then evaluated by solving the Bethe-Salpeter [44, 45] equation (BSE) in the Tamm-Dancoff approximation on top of the ev$GW$ band structure (a summary of the theory is given in the SM [25], Sec. S1). The number of k-points has been fixed to 100 in order to converge the first two singlet excitonic peaks in the absorption spectrum. Finally, we want to specify that results for the excitons are obtained via a dynamical screening calculated using QP eigenvalues for the BSE equation. Detailed numerical parametrization of the

BSE is reported in the SM [25] (Sec. S1).

## III. RESULTS AND DISCUSSION

### A. Electronic structure

While our main focus will be on excitonic properties, it is the quasi-particle band structure that undergoes the topological transition, and understanding its dependence on $n$ provides important insights for our later discussions. Indeed, our aim is to study theoretically the effects of the topological phase transition on the optical properties of polyacene polymers. It is moreover important to note that in order to keep our focus on the essential, intrinsic physics of the transition and its potential impact on excitonic states, we have carried out all of our simulations in vacuum, avoiding further complications due to a surrounding environment. The possible effects of a substrate on the electronic structure is discussed later.

| n | c (Hybrid) | BLA (Hybrid) | $\Delta E$ (Hybrid) | $\Delta E$ (evGW) | $S_I$ (BS) | $E_B$ (BS) | $S_I$-$T_I$ (BS) |
|---|---|---|---|---|---|---|---|
| 3 | 6.89 | 0.215 | 3.48 | 3.33 | 1.84 | 1.49 | 0.49 |
| 5 | 6.92 | 0.210 | 2.35 | 1.53 | 0.77 | 0.76 | 0.30 |
| 7 | 6.91 | 0.098 | 3.31 | 2.78 | 1.66 | 1.12 | 0.62 |

TABLE I. Lattice parameter (c), bond length alternation (BLA), quasiparticle bandgap ($\Delta E$), first singlet energy ($S_I$), binding energy ($E_B$) and first singlet-triplet splitting ($S_I$-$T_I$) for for polyacenes polymers in vacuum as a function of n. All lengths are given in $\AA$, while all energies are given in eV. Hybrid refers to the CAMB3LYP functional [28, 29], evGW to the GW method with self-consistency on the eigenvalues and BS to the Bethe-Salpeter formalism.

In Fig. 2 we report the electronic band-structure obtained for $n = 3, 5, 7$ at the evGW level, together with the HOMO/LUMO wavefunctions both at the center ($k = 0$) and at the border ($k = \pi/c$) of the Brillouin zone. Tab. I reports the result of the single-particle band-gap, obtained via DFT (CAMB3LYP) and DFT+many-body perturbation theory (self-consistent GW on-eigenvalues-only, i.e. evGW) for $n = 3, 5, 7$ in vacuum. All polymers show a direct single-particle band-gap at the edge ($k = \pi/c$) of the Brillouin zone: the gaps decrease from $n = 3$ to $n = 5$, then *increase* for $n = 7$, supporting a picture of a topological phase transition (band closure) between poly-pentacene and poly-heptacene.

We also note that while CAMB3LYP and evGW give very similar gaps for $n = 3$, the band gap for evGW becomes smaller than the CAMB3LYP gap for $n = 5, 7$, suggesting increasing electronic correlations close to the transition: approximate functionals cannot fully take these into account, so more accurate many-body techniques yield larger corrections. The largest deviations occurs for $n = 5$ ($\approx 39\%$), which is the closest to the topological transition (smallest QP gap). Comparison between the band structures computed via CAMB3LYP and evGW for $n = 3 - 7$ are presented in the SM [25] (Sec. S4).

| n | $\Delta$E [eV] (Experimental [22]) | $\Delta$E [eV] (evGW) |
|---|---|---|
| 3 | 1.50 | 3.33 |
| 5 | 0.35 | 1.53 |
| 7 | x | 2.78 |

TABLE II. Quasiparticle bandgap ($\Delta E$) for poly-anthracene (n=3), poly-pentacene (n=5) and poly-heptacene (n=7). Experimental (Exp.) are taken from Ref. [22]while evGW refer to this work.

### B. Screening due to environment

If we compare the evGW estimate of the single-particle band-gap with the experimental values there seems to be a substantial difference (Tab. II). However, our computations are performed in vacuum while from the experimental point of view these polymers are deposited on Au(111) surfaces [22], which acts as a polarization environment, screening long-range interactions and strongly modifying correlation energies [46].

Therefore, we are not taking into account the effects of the environment on the quasiparticle properties. Indeed it has been shown [46, 47] in the case of anthracene and pentacene molecules that, when deposited on metallic surfaces, their quasi-particle band-gap was subjected to a renormalization between 50% and 80% with respect to the gas phase. If we apply such renormalization to our evGW values we find a quasiparticle band-gap between $\sim 2.66$ eV and $\sim 1.67$ eV for poly-anthracene ($n = 3$) and $\sim 1.22$ eV and $\sim 0.77$ eV for poly-pentacene ($n = 5$), which are closer to the experimental results. The final discrepancy with respect to the experimental band-gap might be related to anharmonic effects, which can further reduce the energy difference between the HOMO and LUMO.

This reasoning suggests that the properties of the substrates on which the polymers are grown or deposed could provide another powerful and external control handle. Indeed, the screening from the substrate could substantially reduce the effects of the strong, long-range interactions, allowing for additional modulation of excitonic properties and of the critical acene length $n_c$ at which the topological transition occurs: Cirera *et al.*'s placement of $n = 5$ in the non-trivial phase is likely related to the metallic substrate inducing a gap reduction.

Notice however that neither in Ref. [22] nor in this work anharmonic quantum fluctuations are taken into account: these can play an important role in geometry optimization as well as in the Helmoltz free energy [32, 33, 48], especially close to the quantum critical point.

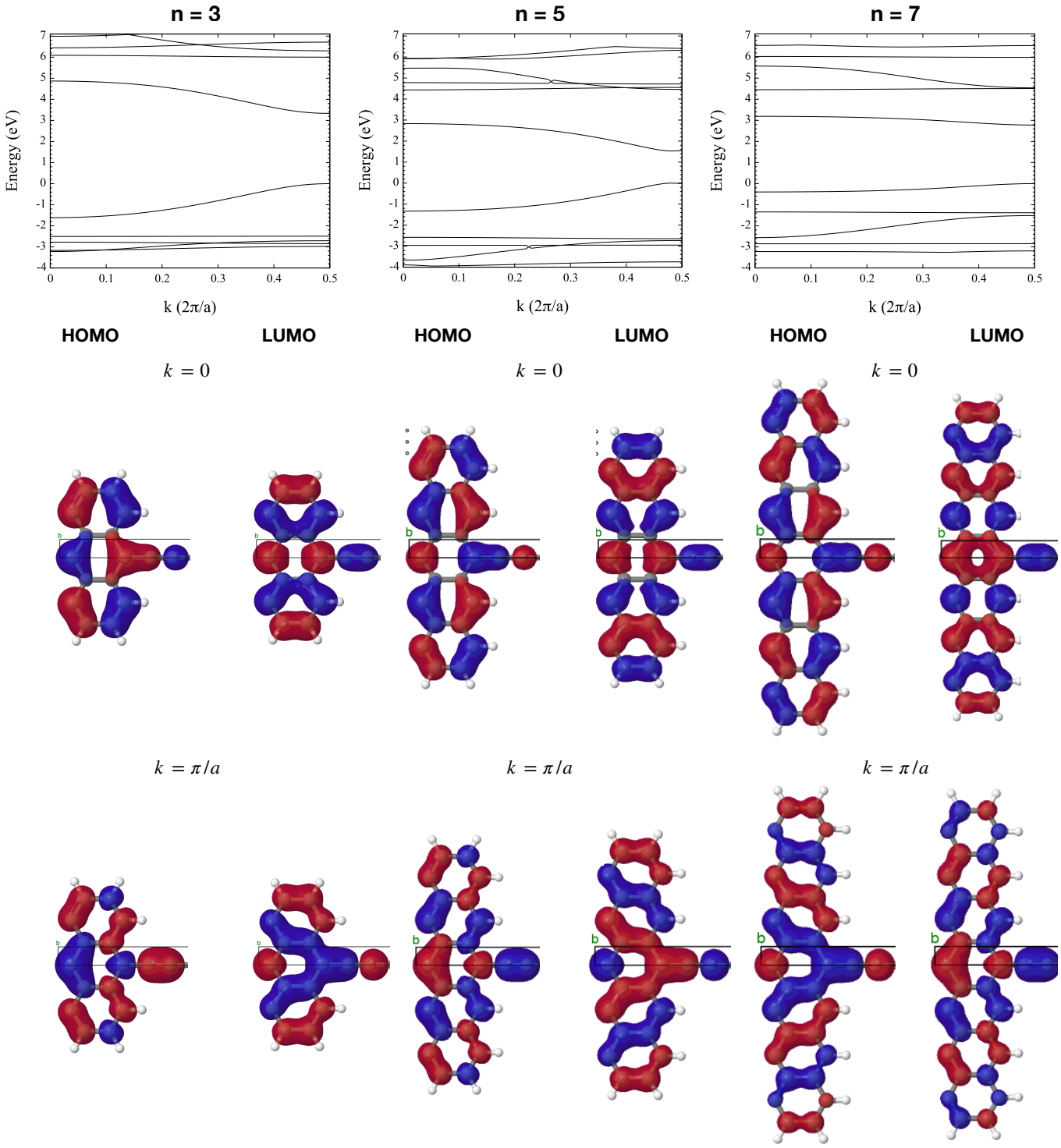


FIG. 2. Self-consistent GW (evGW) quasi-particle bandstucture and HOMOs/LUMOs orbital wavefunctions (with relative phases) at the center ($k = 0$ and at the border ($k = 0.5$) of the Brillouin zone for ethynylene-bridged poly-anthracene (n=3), poly-pentacene (n=5) and poly-heptacene (n=7). Grey (white) spheres represent carbon (hydrogen) atoms.

### C. Exciton wavefunction and band-inversion

In Fig. 3a (left panels) we show the CAMB3LYP valence ($v$), or HOMO, and conduction ($c$), or LUMO, wave functions at the band edges ($k = \pi/c$) for $n = 5$ and $n = 7$, together with (right panel) their first singlet exciton ($S_I$) wavefunctions in both real (with relative phases) and reciprocal space (as contributions coming from states

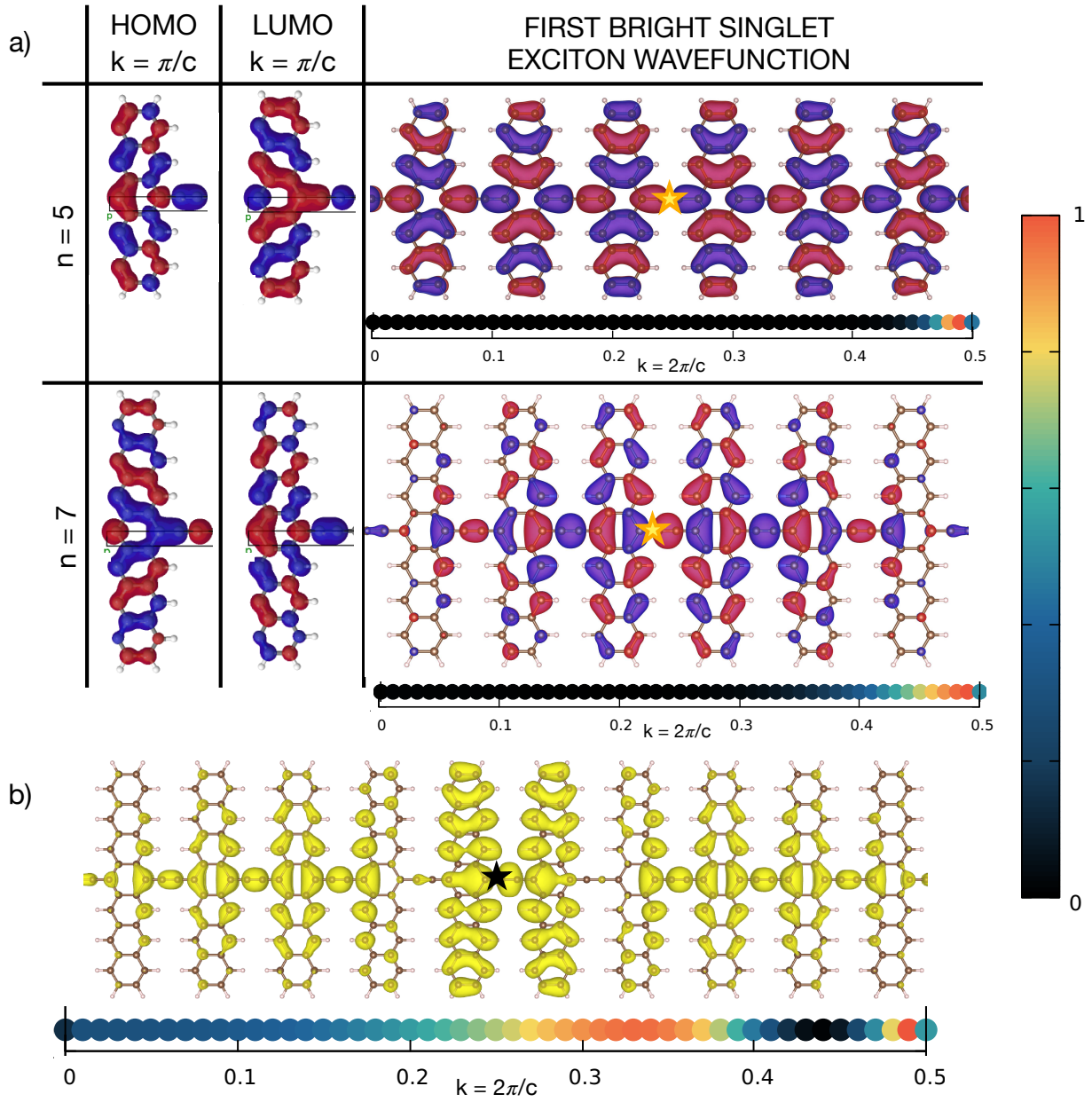


FIG. 3. a) *Left panels:* band-edge ($k = 2\pi/c$) HOMO/LUMO single-particle wave functions (with relative phases) for $n = 5$ and $n = 7$. *Right panel:* exciton wave function in real (with relative phase) and reciprocal space (color bar) of the first bright singlet ($S_I$, see Fig. 4) for $n = 5$ and $n = 7$ at $q = 0$. The yellow star fixes the position of the hole. Due to its large extension, only part of the wave function is shown for $n = 5$. b) $n = 7$, $q = 0$: Real-space (modulus squared) and reciprocal space $S_{III}$ exciton wave function. For both $S_I$ and $S_{III}$, the contributions to the reciprocal space wave functions come from e-h transitions between highest valence and lowest conduction band: black (i.e. 0) in the colorbar means no contribution.

in reciprocal space).

It is clear that the $v$ and $c$ states have *inverted* orbital character when passing from $n = 5$ to $n = 7$. This *band inversion* is the defining feature of the topologically non-trivial phase of the periodic SSH model [1], and occurs *smoothly* across the band structure, i.e. the $c$ ($v$) orbitals of $n = 7$ at $k = 0$ are built from monomer LUMO (HOMO) orbitals and evolve into the inverted order shown in Fig. 3a as $k \to k = \pi/c$ [49]. No band inversion is seen for $n = 3$ and $n = 5$. Thus, in vacuum, the $Z_2$ transition occurs for monomers lengths between $n = 5$ (trivial) and $n = 7$ (nontrivial). This is further supported by the behaviour of the BLA of the bridge atoms (see Tab I), which dramatically reduces from $n = 5 \to n = 7$, indicating the switch from alternating single and triple bonds to a nearly cumulenic double-double bond resonance form. Complete structural characterization can be found in the SM [25] (Sec. S3).

The excitation and binding energies of the lowest (optically bright) singlet ($S_I$) and triplet ($T_I$) excitons are given in Tab I for $n = 3, 5, 7$ . The excitonic gaps follow the same trend as the band structure, as do the large excitonic binding energies ($\sim 0.3 - 0.6$ eV). Strong 1D coulomb interactions generate large singlet-triplet exchange splittings ($\sim 0.3/0.6$ eV) in all polymers (Tab. I). Strikingly, the optical gap for $n = 5$ is dramatically reduced (0.77 eV, c.f. 1.8 eV in molecular crystals), and the strong increase in the $S_I$ binding energies from $n = 5 \rightarrow n = 7$ (Tab. I) implies a transition from Mott-Wannier to Frenkel excitons. Indeed the Bohr's radius of $S_I$ goes from $\sim 76$ Å (i.e. $\sim 11$ unit cells) to $\sim 28$ Å (i.e. $\sim 4$ unit cells) when passing from $n = 5$ to $n = 7$. The change in localization of the excitonic wave function is clearly seen in both real and reciprocal space in Fig. 3a (right panel).

As the k-space distribution of e-h transitions in both $S_I$ states is confined to the band edges, the exciton wave functions closely resemble the conduction band states at $k = \pi/c$, and thus also show band inversion as $n = 5 \rightarrow n = 7$. Indeed, the exciton wave function receives contributions from single-particle orbitals taking part to the excitation and, as a consequence of the band inversion at the border of the Brillouin zone, we can observe as well a corresponding modification of the orbital character in the exciton wavefunction in real space.

However, a more dramatic effect of topological band inversion is shown in Fig.3b, which shows the third bright excition ($S_{III}$) for $n = 7$. Here, we observe a very broad distribution of e-h transitions in the $k$-space wave function, whose width is larger than the region over which the band inversion occurs. This leads to contributions from single particle transitions in *both* the inverted and non-inverted regions of the $c/v$ bands. As a consequence, we observe a mixture of HOMO/LUMO states in the exciton wavefunction. These potentially measureable orbital textures are always absent in the topologically-trivial $n = 3$ and $n = 5$ polymers as no band exchange happens in their electronic structure. Representations of all singlet and triplet exciton wavefunctions for $n = 3, 5, 7$ is given in the SM [25] (Sec. S6).

### D. Exciton dispersions and singlet fission

Fig. 4 compares the exciton dispersions $E^{\lambda}(q)$ for $n = 5$ and $n = 7$ as a function of the center-of-mass momentum q. Singlet excitons are optically spin-allowed, and have been plotted to take into account their *generalized optical strength*:

$$f_{\lambda}(q) = \left| \sum_{c,v,k} A^{\lambda}_{c,v}(k,q) \langle c, k+q | \mathbf{D} | v, k \rangle \right|^2 \qquad (1)$$

where $|c, k+q\rangle$ ($|vk\rangle$) is the Bloch wave function for an electron (hole) with momentum $k+q$ ($k$) on band $c$ ($v$), $\mathbf{D}$ is the electric dipole operator (here, aligned along polymer repeat axis) and $A^{\lambda}_{c,v}(k,q)$ is the amplitude of a given electron-hole transition in the excitonic ($\lambda$) wave function in $k$ space.

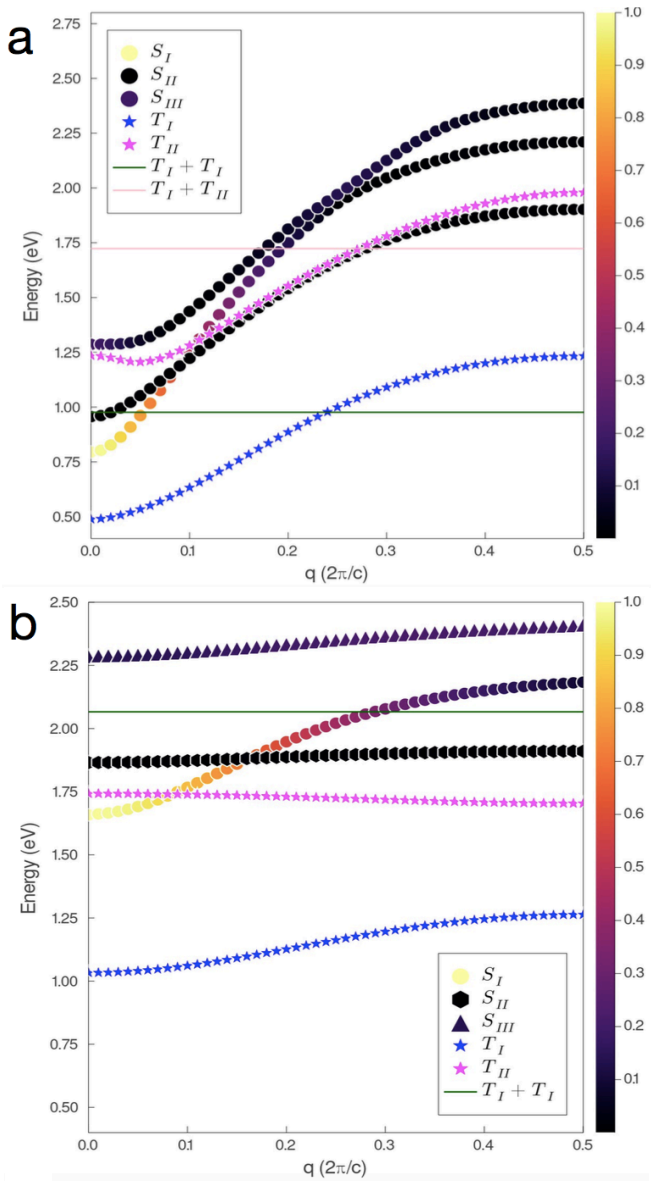


FIG. 4. Exciton dispersions for $n = 5$ (a) and $n = 7$ (b) showing the energy threshold for triplet pair creation (horizontal lines). Singlet exciton dispersions are coloured according to their normalized optical oscillator strength (color bar), with the brightest state having unit strength.

For $n = 5$, we find a rather congested spectrum containing both bright and dark singlet excitons, as well as two triplet bands. Notably, the lowest bright singlet exciton ($S_I$) is extraordinarily dispersive and remains 'optically' active over more than 60% of its bandwidth (1.6 eV, c.f. $\approx 0.1$ eV in monomer films [50]). Note that only states within the optical light cone can actually be

excited by light, but the finite optical transition dipole moments of larger-$q$ excitons will still be important for processes such as inter-polymer förster energy transfer and near-field, nano optical experiments on intrachain photodynamics [51, 52]. Triplet excitons are also highly dispersive, with band widths of $\approx 0.7$ eV, c.f. $\approx 0.03$ eV in films [50]. On the other side of the topological transition ($n = 7$), the exciton dispersions become significantly flatter, matching the underlying band structure (Fig.2). However, the bright singlets maintain their oscillator strengths over a much larger momentum range due to their Frenkel-like nature (small Bohr radius).

Acene-based films and crystals are also known to undergo the process of singlet fission (SF) [50, 53], which allows a singlet exciton to decay into a pair of spin-entangled triplet excitons [54] and could be used to increase the efficiency of organic photovoltaics [55]. Here, we find that the strong dispersion of the $n = 5$ polymer permits - on energetic grounds - the decay of $S_I$ at finite-$q$ into *both* $T_IT_I$ *and* excited $T_IT_{II}$ triplet pairs (see Fig.4) [54]: although the $q = 0$ $S_I$ state lies below the threshold energy for SF ($\approx 2 \times E_{T_I}$), as shown on Fig.4, its rapid dispersion creates a large, energetically alllowed phase space for SF at finite momentum. Finite-$q$ SF has previously been shown to be an effective mechanism in pentacene ($n = 5$) thin films [50], even though the joint phase space is much smaller, due to the narrow dispersion of singlet excitons in films [50]. Strikingly, the $n = 5$ polymer also permits ( on energetic grounds) the decay of $S_I$ at large-$q$ into an excited $T_IT_{II}$ triplet pair (Fig.4). Recently, Pandya *et al.* have shown that optical excitation of a $(T_IT_I) \rightarrow (T_IT_n)$ transition induces spatial separation of the tightly bound triplet pairs that form the lowest excited state of blue polydiacetylenes, suggesting that the new SF pathway available in the $n = 5$ polymer could also spontaneously generate 'free' triplets pairs that preserve their germinate spin entanglement across real space [54].

Another critical aspect of SF is the matrix element for the conversion of a singlet Frenkel-like exciton, which - in acenes - is thought to arise via a super-exchange mechanism involving a higher-lying 'charge transfer' singlet exciton. While determination of SF rates is beyond the scope of this work (see Ref. [50]), we do point out that the matrix elements for SF typically involve (virtual) super-exchange coupling via a higher-lying charge-transfer exciton [56]. Indeed, this matrix element takes the generic form:

$$\chi_{SF} = (M_{S_I}^{S_n} M_{S_n}^{TT})(\Delta E_{S_I S_n})^{-1} \qquad (2)$$

where $M_x^y$ is a Coulombic transition amplitude between states $x$ and $y$ that are separated in energy by $\Delta E_{xy}$. As shown in Sec. S6, the $S_{III}$ state in polypentacene (i.e. $n = 5$) has strong charge-transfer character, corresponding to a large $M_{S_{III}}^{TT}$, and strongly mixes with $S_I$ near the avoided crossing ($\Delta E_{S_I S_{III}} \approx 0$). Consequently, a large super-exchange $\chi_{SF}$ could be also be expected above threshold, leading to concomitantly large SF rates. We also note that, for $n = 5$, $S_{III}$ at $q = 0$ is already above threshold and is optically bright, permitting *direct* SF from this CT state [56].

On the other side of the topological transition ($n = 7$), the larger relative energy of the $T_I$ states reduces the phase space for finite-$q$ SF, although the $S_{III}$ band remains above threshold for all momenta. We also note that the bright singlets maintain their oscillator strengths over a much larger momentum range for $n = 7$ with respect to $n = 5$, due to the smaller excitonic Bohr radius. However, the key change of relevance for SF is the effect of band inversion on the SF matrix elements: as SF matrix elements are constructed from the coherent summation of Coulombic scattering amplitudes of electrons and holes [50], this 'texture' in the electron density could lead to strong interference effects, which - to the best of our knowledge - have not previously been identified or studied. Such topologically induced interference effects would also radically affect the matrix elements for any finite-momentum scattering processes, such as the exciton-phonon interaction and related properties, e.g. resonance Raman spectra.

### E. Negatively dispersive excitons

Another interesting feature in Fig. 4 is the existence of *negatively* dispersing $T_{II}$ excitons. For $n = 5$ this negative dispersion is confined to a small region around $q = 0$, while for $n = 7$ it extends across the entire band, decreasing across the band by $\approx 40$ meV ($K_BT \approx 25$ meV at 298K), so that phonon scattering should *spontaneously* relax these excitons into stable finite-momenta states. At low temperatures, this could significantly modify the mechanism of triplet transport. A weak negative dispersion of the $T_{II}$ in a pentacene crystal was also observed, though not analysed, in Ref. [50].

With a view to understanding and controlling these anomalous dispersions, Fig.5a compares the $k$-space distributions of e-h transitions in the $T_{II}$ state on the $n = 7$ quasiparticle band structure. At $q = 0$, the $T_{II}$ state is built by e-h pairs clustered around the band edge and zone center, and at $q = \pi/c$ the dominant transitions lie in the centre of the band[57]. According to the effective Bethe-Salpeter Hamiltonian, the energy of the triplet exciton states contains two contributions: the (non-interacting) kinetic energy of the e-h quasiparticles and the matrix element between the conduction $c$ and valence $v$ band of the Fourier transform of the screened direct Coulomb interaction $K^X_{\substack{cvk \\ c'v'k'}}$ at k-points $k$ and $k' = k + q$. Due to the flatness of the band structure for poly-heptacene, there is essentially no change in the carrier's kinetic energy as $T_{II}(q = 0) \rightarrow T_{II}(q = \pi/c)$, whereas this normally provides a strong, positive contribution to the exciton dispersion, as it does for polypentacene.

At the same time, the direct Coulomb interaction ma-

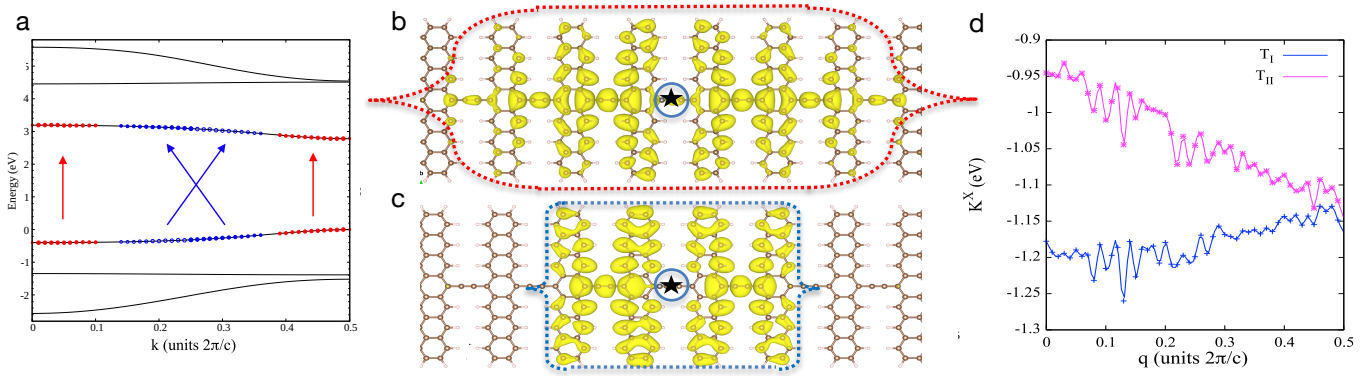


FIG. 5. Poly-heptacene (n=7): (a) single-particle transitions responsible for $T_{II}$ at $q = 0$ (red) and $q = \pi/c$ (blue) on top of the folded band structure in the irreducible first Brillouin zone; (b-c) Modulus squared of the exciton wave functions for $T_{II}$ at $q = 0$ (b) and $q = \pi/c$ (c) showing contraction of the exciton at finite momentum. Holes are localized at circled position; (d) Screened direct Coulomb interaction $K^X$ averaged over triplet eigenfunctions as a function of $q$, obtained with Yambopy.

trix element that mixes e-h transitions in the excitonic wave function arises from a screened $q$-dependent interaction. Fig. 5d shows the screened $q$-dependent direct interaction averaged over triplet states for the $n = 7$:

$$K^X(q) = \sum_{\substack{cvk \\ c'v'k'}} (A^{\lambda}_{c',v'}(k',q))^* A^{\lambda}_{c,v}(k,q) K^X_{\substack{cvk \\ c'v'k'}} \qquad (3)$$

showing that $K^X(q)$ is a continuously *decreasing* function of $q$ for $T_{II}$, i.e. the binding energy of the exciton becomes *greater* at the band edge. Combined with the neutral change in carrier Kinetic energy (K.E.) - which is induced by the flat bands that appear above the topological transition - we then see that the negative dispersion arises from reduced screening at short wavelengths (large $q$). This interpretation is visualized directly in Fig.5b&c, where the shrinkage (increased binding energy/decreasing Bohr radius) of the exciton can be seen in the real-space wave function as $q \to \pi/c$.

Thus, it is the flat bands that *must* appear above the topological transition (the disconnected dimer limit, in the SSH model) that promote anomalous exciton dynamics. We also note that negative dispersions in molecular acene crystals have previously been reported for low-lying singlet excitons, and were shown to arise from mixing (level repulsion) with higher-lying CT excitons [58, 59]. While the congested spectrum for $n = 5$ may partially promote a similar mechanism in the non-monotonic dispersion of $T_{II}$ and the rather flat $S_{III}$, the CT bands are well separated for $n = 7$, and the *shrinkage* of the wave function at the band edge is inconsistent with growing admixtures of CT states with *enhanced* e-h separations.

## IV. CONCLUSION

In conclusion, we have shown that the topological transition occurring in ethynylene-bridged acene polymers offers extreme tunability of optoelectronic properties, and we believe that the rather general mapping between $1D$ molecule-bridge structures and the SSH model should extend this tunability to many other organic constructs [22]. Additionally, the properties of the substrates on which the polymers are grown or deposed could provide another powerful and external control handle. Indeed, the screening from the substrate could substantially reduce the effects of the strong, long-range vacuum interactions native to organics, allowing for additional modulation of excitonic properties and - most importantly - of the critical acene length $n_c$ at which the topological transition occurs. Additionally, based on the findings of previous work on carbynes [32] and finite-sized acene polymers [23], the cross-over from acetylenic to cumulenic bridging at the transition suggests that phonons and anharmonicity could also play an important, temperature-dependent role in closing the charge gap, and this will be discussed in future work.

## ACKNOWLEDGMENTS

The authors acknowledge support from the ANR project ACCEPT (Grant No. ANR-19-CE24-0028). This work was granted access to the HPC resources of IDRIS, CINES and TGCC under the allocation 2021-A0100912417 made by GENCI. MC acknowledges PRACE (Grant no. 2021240020) for awarding him access to irene Rome in France. D. R. thanks D. Varsano and F. Paleari for fruitful dicussion on the GW+BSE computations. The authors acknowledge M. Casula for fruitful discussion on the possible insurgence of an antiferromagnetic groundstate. The data that supports the findings of this study are available from the corresponding author on reasonable request.

[1] D. Vanderbilt, *Berry phases in electronic structure theory: electric polarization, orbital magnetization and topological insulators* (Cambridge University Press, 2018).
[2] O. Breunig and Y. Ando, Nature Reviews Physics , 1 (2021).
[3] T. Cao, F. Zhao, and S. G. Louie, Physical review letters **119**, 076401 (2017).
[4] J. Li, S. Sanz, N. Merino-Díez, M. Vilas-Varela, A. Garcia-Lekue, M. Corso, D. G. de Oteyza, T. Frederiksen, D. Peña, and J. I. Pascual, Nature communications **12**, 1 (2021).
[5] F. Zhao, T. Cao, and S. G. Louie, Physical review letters **127**, 166401 (2021).
[6] B. Seradjeh, J. E. Moore, and M. Franz, Phys. Rev. Lett. **103**, 066402 (2009).
[7] D. I. Pikulin and T. Hyart, Phys. Rev. Lett. **112**, 176403 (2014).
[8] J. C. Budich, B. Trauzettel, and P. Michetti, Phys. Rev. Lett. **112**, 146405 (2014).
[9] W. T. Fuhrman, J. Leiner, P. Nikolić, G. E. Granroth, M. B. Stone, M. D. Lumsden, L. DeBeer-Schmitt, P. A. Alekseev, J.-M. Mignot, S. M. Koohpayeh, P. Cottingham, W. A. Phelan, L. Schoop, T. M. McQueen, and C. Broholm, Phys. Rev. Lett. **114**, 036401 (2015).
[10] W. K. Park, L. Sun, A. Noddings, D.-J. Kim, Z. Fisk, and L. H. Greene, Proceedings of the National Academy of Sciences **113**, 6599 (2016), https://www.pnas.org/doi/pdf/10.1073/pnas.1606042113.
[11] A. Blason and M. Fabrizio, Phys. Rev. B **102**, 035146 (2020).
[12] G. Xu, T. Zhou, B. Scharf, and I. Žutić, Phys. Rev. Lett. **125**, 157402 (2020).
[13] Y. H. Kwan, Y. Hu, S. H. Simon, and S. A. Parameswaran, Phys. Rev. Lett. **126**, 137601 (2021).
[14] J. Knolle and N. R. Cooper, Phys. Rev. Lett. **118**, 096604 (2017).
[15] L. Du, X. Li, W. Lou, G. Sullivan, K. Chang, J. Kono, and R.-R. Du, Nature Communications **8**, 1971 (2017).
[16] H.-H. Kung, A. P. Goyal, D. L. Maslov, X. Wang, A. Lee, A. F. Kemper, S.-W. Cheong, and G. Blumberg, Proceedings of the National Academy of Sciences **116**, 4006 (2019), https://www.pnas.org/doi/pdf/10.1073/pnas.1813514116.
[17] D. Varsano, M. Palummo, E. Molinari, and M. Rontani, Nature Nanotechnology **15**, 367 (2020).
[18] T. Cao, M. Wu, and S. G. Louie, Phys. Rev. Lett. **120**, 087402 (2018).
[19] X. Zhang, W.-Y. Shan, and D. Xiao, Phys. Rev. Lett. **120**, 077401 (2018).
[20] A. Köhler and H. Bässler, *Electronic processes in organic semiconductors: An introduction* (John Wiley & Sons, 2015).
[21] H. Bronstein, C. B. Nielsen, B. C. Schroeder, and I. McCulloch, Nature Reviews Chemistry **4**, 66 (2020).
[22] B. Cirera, A. Sánchez-Grande, B. de la Torre, J. Santos, S. Edalatmanesh, E. Rodríguez-Sánchez, K. Lauwaet, B. Mallada, R. Zbořil, R. Miranda, O. Gröning, P. Jelínek, N. Martín, and D. Ecija, Nature Nanotechnology **15**, 437 (2020).
[23] H. González-Herrero, J. Mendieta-Moreno, S. Edalatmanesh, J. Santos, N. Martín, D. Écija, B. de la Torre, and P. Jelinek, Adv. Mater. **33**, 2104495 (2021).
[24] J.-M. André, B. Champagne, E. A. Perpète, and M. Guillaume, International Journal of Quantum Chemistry **84**, 607 (2001).
[25] See Supplemental Material at http://link.aps.org/supplemental/xxx for: BSE formalism and numerical details, mapping to the SSH model, structural properties, CAMB3LYP vs. evGW bandstructures, antiferromagnetic groundstate and exciton wavefunctions.
[26] M. Ratner, Nature nanotechnology **8**, 378 (2013).
[27] M. K. Man, J. Madéo, C. Sahoo, K. Xie, M. Campbell, V. Pareek, A. Karmakar, E. L. Wong, A. Al-Mahboob, N. S. Chan, *et al.*, Science Advances **7**, eabg0192 (2021).
[28] T. Yanaia, D. P. Tewb, and N. C. Handy, Chemical Physics Letters **393**, 51 (2004).
[29] Y. Tawada, T. Tsuneda, and S. Yanagisawa, J. Chem. Phys. **120**, 8425 (2004).
[30] R. Dovesi, R. Orlando, A. Erba, C. M. Zicovich-Wilson, B. Civalleri, S. Casassa, L. Maschio, M. Ferrabone, M. D. L. Pierre, P. D'Arco, Y. Noël, M. Causà, M. Rérat, and B. Kirtman, International Journal of Quantum Chemistry **114**, 1287 (2014).
[31] R. Dovesi, A. Erba, R. Orlando, C. M. Zicovich-Wilson, B. Civalleri, L. Maschio, M. Rérat, S. Casassa, J. Baima, S. Salustro, and B. Kirtman, WIREs Comput Mol Sci. **8**, 1360 (2018).
[32] D. Romanin, L. Monacelli, R. Bianco, I. Errea, F. Mauri, and M. Calandra, J. Phys. Chem. Lett. **12**, 10339 (2021).
[33] D. Romanin and M. Calandra, Carbon Trends **9**, 100207 (2022).
[34] D. V. Oliveira, J. Laun, M. F. Peintinger, and T. Bredow, Journal of Computational Chemistry **40**, 2364 (2019).
[35] R. E. Blackwell, F. Zhao, E. Brooks, J. Zhu, I. Piskun, S. Wang,A. Delgado,Y.-L. Lee,S. G. Louie, and F. R. Fischer, Nature **600**, 647-652 (2021).
[36] R. Meena, G. Li, and M. Casula, J. Chem. Phys. **156**, 084112 (2022).
[37] A. Marini, C. Hogan, M. Grüning, and D. Varsano, Computer Physics Communications **8**, 180 (2009).
[38] D. Sangalli, A. Ferretti, H. Miranda, C. Attaccalite, I. Marri, E. Cannuccia, P. Melo, M. Marsili, F. Paleari, A. Marrazzo, G. Prandini, P. Bonfà, M. O. Atambo, F. Affinito, M. Palummo, A. Molina-Sánchez, C. Hogan, M. GrÃŒning, D. Varsano, and A. Marini, Journal of Physics: Condensed Matter **31**, 325902 (2019).
[39] H. N. Rojas, R. W. Godby, and R. J. Needs, Phys. Rev. B **74**, 10 (1995).
[40] P. Giannozzi, S. Baroni, N. Bonini, M. Calandra, R. Car, C. Cavazzoni, D. Ceresoli, G. L. Chiarotti, M. Cococcioni, I. Dabo11, A. D. Corso, S. de Gironcoli, S. Fabris, G. Fratesi, R. Gebauer, U. Gerstmann, C. Gougoussis, A. Kokalj, M. Lazzeri, L. Martin-Samos, N. Marzari, F. Mauri, R. Mazzarello, S. Paolini, A. Pasquarello, L. Paulatto, C. Sbraccia1, S. Scandolo, G. Sclauzero, A. P. Seitsonen, A. Smogunov, P. Umari, and R. M. Wentzcovitch, Journal of Physics: Condensed Matter **21**, 395502 (2009).
[41] P. Giannozzi, O. Andreussi, T. Brumme, O. Bunau, M. B. Nardelli, M. Calandra, R. Car, C. Cavazzoni,

D. Ceresoli, M. Cococcioni, N. Colonna, I. Carnimeo, A. D. Corso, S. de Gironcoli, P. Delugas, R. A. D. Jr., A. Ferretti, A. Floris, G. Fratesi, G. Fugallo, R. Gebauer, U. Gerstmann, F. Giustino, T. Gorni, J. Jia11, M. Kawamura, H.-Y. Ko, A. Kokalj, E. Küçükbenli, M. Lazzeri, M. Marsili, N. Marzari, F. Mauri, N. L. Nguyen, H.-V. Nguyen, A. O. de-la Roza, L. Paulatto, S. Poncé, D. Rocca, R. Sabatini, B. Santra, M. Schlipf, A. P. Seitsonen, A. Smogunov, I. Timrov, T. Thonhauser, P. Umari, N. Vast, X. Wu, and S. Baroni, Journal of Physics: Condensed Matter **29**, 465901 (2017).

[42] C. A. Rozzi, D. Varsano, A. Marini, E. K. U. Gross, and A. Rubio, Phys. Rev. B **73**, 205119 (2006).

[43] C. Faber, P. Boulanger, I. Duchemin, C. Attaccalite, and X. Blase, J. Chem. Phys. **139**, 194308 (2013).

[44] G. Strinati, Rivista del Nuovo Cimento **11**, 12 (1988).

[45] G. Bussi, Physica Scripta **2004**, 141 (2003).

[46] J. B. Neaton, M. S. Hybertsen, and S. G. Louie, Phys. Rev. Lett. **97**, 216405 (2006).

[47] F. Amy, C. Chan, and A. Kahn, Org. Electron. **6**, 85 (2005).

[48] L. Monacelli, R. Bianco, M. Cherubini, M. Calandra, I. Errea, and F. Mauri, J. Phys.: Condens. Matter **33**, 363001 (2021).

[49] Modifications of the HOMO (LUMO) monomer orbitals due to the $\pi$ orbitals of the bridge are present in all cases.

[50] S. Refaely-Abramson, H. Felipe, S. G. Louie, and J. B. Neaton, Physical Review Letters **119**, 267401 (2017).

[51] A. Davoody and I. Knezevic, in *Physics, Simulation, and Photonic Engineering of Photovoltaic Devices IV*, Vol. 9358 (SPIE, 2015) pp. 138–145.

[52] B. Hanewinkel, A. Knorr, P. Thomas, and S. Koch, Physical Review B **60**, 8975 (1999).

[53] M. B. Smith and J. Michl, Chemical reviews **110**, 6891 (2010).

[54] R. Pandya, Q. Gu, A. Cheminal, R. Y. Chen, E. P. Booker, R. Soucek, M. Schott, L. Legrand, F. Mathevet, N. C. Greenham, *et al.*, Chem **6**, 2826 (2020).

[55] M. B. Smith and J. Michl, Annual review of physical chemistry **64**, 361 (2013).

[56] T. C. Berkelbach, M. S. Hybertsen, and D. R. Reichman, The Journal of chemical physics **138**, 114102 (2013).

[57] Concerning $q = 0.5$ (i.e. $q = \pi/c$, in units of $2\pi/c$), in Fig. 5a light blue (dark blue) dots represent electrons excited from band $v$ at states $0.15 \leq k < 0.25$ ($0.25 < k \leq 0.35$) to band $c$ at states $0.25 < k \leq 0.35$ ($0.15 \leq k < 0.25$) in the irreducible first Brillouin zone (i.e. $0.0 \leq k \leq 0.5$).

[58] F. Roth, M. Nohr, S. Hampel, and M. Knupfer, EPL (Europhysics Letters) **112**, 37004 (2015).

[59] P. Cudazzo, F. Sottile, A. Rubio, and M. Gatti, Journal of Physics: Condensed Matter **27**, 113204 (2015).